RSC Advances

PAPER

View Article Online
View Journal | View Issue

Cite this: RSC Adv., 2017, 7, 11312

A highly selective "ON–OFF" probe for colorimetric and fluorometric sensing of Cu^{2+} in water†

Barnali Naskar,[a] Ritwik Modak,[a] Dilip K. Maiti,[a] Antonio Bauzá,[b] Antonio Frontera,[b] Pulak Kumar Maiti,[c] Sukhendu Mandal[c] and Sanchita Goswami*[a]

Received 18th November 2016
Accepted 7th February 2017

DOI: 10.1039/c6ra27017d

rsc.li/rsc-advances

We present herein a diformyl phenol based probe, 3-({3-[2,3-dihydroxy-propylimino-methyl]-2-hydroxy-5-methyl-benzylidene}-amino)-propane-1,2-diol (H_5**dpm**), as a colorimetric and fluorometric chemosensor for selective detection of Cu^{2+} in aqueous solution under physiological conditions. This simple system produces a colorimetric change enabling naked eye detection as well as on–off fluorescence response towards Cu^{2+} in an aqueous medium with a detection limit of 11.2 nM. To further demonstrate the utility of H_5**dpm**, we next explored the application of H_5**dpm** for imaging Cu^{2+} in Vero cells. The attractive imaging properties of the H_5**dpm** probe will open up avenues for molecular imaging and biomedical applications.

1. Introduction

Cu^{2+} is recognized as the third most abundant metal ion after Fe^{3+} and Zn^{2+} and it plays a vital role in several biological processes such as hemoglobin biosynthesis, bone development and nerve function regulation.[1–15] However, inadequate as well as excessive uptake of Cu^{2+} in biological systems can cause disorders associated with neurodegenerative diseases, such as Alzheimer's disease, Menke's disease and Wilson's disease.[16–41] Moreover, in a natural environment, copper is also considered as a significant pollutant due to its high toxicity.[42–45]

Among the powerful tools available for Cu^{2+} detection are atomic absorption spectrometry, quantum dot based assays, inductively coupled mass spectrometry (ICPMS), inductively coupled plasma-atomic emission spectrometry (ICP-AES) and electrochemical techniques.[46–48] However, these methods have limitations that require sophisticated instrumentation, large sample amounts and time consuming techniques. On the contrary, optical sensors, which involve naked-eye detection and/or fluorescence intensity change, have attracted great research interest as these provide quick, non-destructive and selective results.

Owing to the significant physiological relevance and associated biomedical implications, development of selective and sensitive colorimetric and/or fluorogenic chemosensors for Cu^{2+} in biological and environmental samples has captured the attention of many research groups. However, the challenge lies in the development of sensors which are biocompatible and functional in the physiological environment. The versatility of a chemosensor depends upon its working ability in an aqueous environment and at physiological pH, which enables its utilization in *in vivo* applications. A considerable number of fluorescence based chemosensors have been reported for Cu^{2+} in the past few years.[49–55] However, a couple of them possess disadvantages such as complicated synthetic procedures, unimpressive detection limit, use of organic solvents and interference from other associated metal ions.[46,54,56–58] Most of the techniques for accurate and selective detection of Cu^{2+} are based on chemosensors that undergo a fluorescence intensity quenching (turn-OFF) in presence of analyte.[55,59–62]

As part of our interest in designing fluorescence sensors for cations,[63] we have decided to target the construction of keto–enol tautomerism based chemosensors because tautomerism facilitates electron transfer processes responsible for sensing and their ability to bind the analyte through a specific tautomer makes them an interesting class of probes. Diformyl phenol derivatives have been widely used as fluorescence chemosensors on account of their excellent luminescence properties.[64–68] To the best of our knowledge, limited work has been carried out in the development of diformyl phenol based probes for selective colorimetric sensing of Cu^{2+} and only two examples are there that represent quenching based detection of Cu^{2+} (ESI Chart 1†).[58,69] Furthermore, involvement of tautomeric equilibrium has not been explored till date.

[a]Department of Chemistry, University of Calcutta, 92, A.P.C. Road, Kolkata-700 009, India. E-mail: sgchem@caluniv.ac.in; goswami.sanchita@gmail.com

[b]Departament de Química, Universitat de les IllesBalears, Crta. deValldemossa km 7.5, 07122 Palma de Mallorca, Baleares, Spain

[c]Department of Microbiology, University of Calcutta, 35, Ballygunge Circular Road, Kolkata, India

† Electronic supplementary information (ESI) available: FT-IR, ESI-MS, ^1H and ^{13}C of H_5**dpm**, photophysical characterization of H_5**dpm** and Cu(II), theoretical data. CCDC 1529126. For ESI and crystallographic data in CIF or other electronic format see DOI: 10.1039/c6ra27017d

Bearing these in mind, we have decided to evaluate a new diformyl phenol based sensing system, **H_5dpm**, generated by condensation of 2,6-diformyl-4-methylphenol and 3-amino-1,2-propanediol. It can be successfully used for nanomolar sensing of Cu^{2+} in aqueous solution (Tris buffer, pH = 7.4) *via* a turn-off fluorescence response. Furthermore, fluorescence imaging experiments of Cu^{2+} in living Vero cells demonstrated its value of practical application in biological systems.

2. Experimental section

2.1. Materials and physical methods

3-Amino-1,2-propanediol, $Zn(OAc)_2\cdot 2H_2O$, $Cu(NO_3)_2\cdot 3H_2O$ and high-purity Tris-buffer were purchased from Sigma-Aldrich. Buffer was prepared using triple distilled water. Solvents used for spectroscopic studies and for the syntheses were purchased from commercial sources and used as received. Elemental analyses for C, H and N were performed on a Perkin-Elmer 2400 II analyzer. The FT-IR spectra were recorded from KBr pellets in the range of 400–4000 cm^{-1} on a Perkin-Elmer Spectrum 100 spectrometer. ^{1}H and ^{13}C-NMR spectra were recorded with TMS as internal standard on a Bruker, AV 300 Supercon Digital NMR system. The ESI-MS were recorded on Qtof Micro YA263 mass spectrometer. A Systronics digital pH meter (model 335) was used to measure the pH of the solution, and the adjustment of pH was done using either 50 mM HCl or NaOH solution. The absorption and emission spectra were recorded on a Hitachi UV-vis U-3501 spectrophotometer and Perkin-Elmer LS55 fluorimeter, respectively.

3. Syntheses and characterisation

3.1. Synthesis of probe 3-({3-[2,3-dihydroxy-propylimino)-methyl]-2-hydroxy-5-methyl-benzylidene}-amino)-propane-1,2-diol (H_5dpm)

The synthesis of 4-methyl-2,6-diformylphenol(2-hydroxy-5-methyl-benzene-1,3-dicarbaldehyde) was accomplished by a method adapted from literature procedure.[70] A methanol (15 mL) solution of 4-methyl-2,6-diformylphenol (0.328 g, 2 mmol) was taken and 3-amino-1,2-propanediol (0.375 g, 4 mmol) in 15 mL methanol solution was added to it dropwise with continuous stirring at room temperature. Then the resulting reaction mixture was refluxed for 6.0 h. The solution was filtered, concentrated on a rota-evaporator to get (92%) an oily orange liquid compound which was recrystallised from methanol for purification and was used throughout the experiment and characterisation. Anal. calcd for $C_{15}H_{22}N_2O_5$: C, 58.05; H, 7.15; N, 9.03; found: C, 58.03; H, 7.16; N, 9.02; ^{1}H-NMR (300 MHz, DMSO-d_6) δ_H: 14.3 (1H), 8.59 (s, 2H), 7.56 (s, 2H), 4.83 (d, J = 5.2 Hz, 4H), 3.82 (m, 4H), 3.54 (m, 6H), 3.31 (3H); ^{13}C-NMR (300 MHz, DMSO-d_6) δ_C: 161.19, 160.0, 131.76, 125.34, 120.56, 70.54, 63.40, 62.08, 48.12, 39.84, 19.41 (ESI Fig. S1†); selected FT-IR data (KBr, cm^{-1}) $\nu_{(OH)}$ = 3413 cm^{-1}, $\nu_{(C=N)}$ = 1646 cm^{-1} (ESI Fig. S3†). ESI-MS m/z, ion: 311.1676, [**H_5dpm** + H]$^+$, $C_{15}H_{23}N_2O_5$ (ESI Fig. S4†).

3.2. Synthesis of complex [Zn–H_5dpm] (1)

A methanolic solution (10 mL) of $Zn(OAc)_2\cdot 2H_2O$ (0.439 g, 2 mmol) was added drop wise to a methanolic solution (10 mL) of **H_5dpm** (0.310 g, 1 mmol) with constant stirring and continued for further 2 h. Then, a methanolic solution (5 mL) of NH_4SCN (0.076 g, 1 mmol) was added, and the resulting solution was stirred for 4 h. The greenish yellow solution was filtered and kept for slow evaporation. Crystals of complex **1**, suitable for X-ray structure, were obtained at ambient temperature within 3 days. Yield: 81%. Anal. calcd for $C_{20}H_{27}N_3O_9SZn_2$: C, 38.98; H, 4.42; N, 6.82. Found: C, 38.97; H, 4.41; N, 6.80. Selected FT-IR data (KBr, cm^{-1}), (ESI Fig. S3†) $\nu_{(OH)}$ = 3367.84 cm^{-1}, $\nu_{(C=N)}$ = 1638.44 cm^{-1}, $\nu_{(SCN)}$ = 2078.62 cm^{-1}, ESI-MS m/z, ion: 557.0260, [**H_4dpm** + $Zn_2(OAC)_2$]$^+$, $C_{19}H_{27}N_2O_9Zn_2$ (ESI Fig. S4†).

3.3. Synthesis of complex [Cu–H_5dpm] (2)

To a solution of $Cu(NO_3)_2\cdot 3H_2O$ (0.483 g, 2 mmol) in methanol (10 mL) was added drop wise a methanol solution of **H_5dpm** (0.310 g, 1 mmol) with constant stirring for further 1 h. The mixture was refluxed for 2 h. The green solution was filtered and kept for slow evaporation. After a few days, green crystalline compound were obtained. Yield: 78%. Anal. calcd for $C_{15}H_{19}N_2O_5Cu_2$: C, 41.47; H, 4.41; N, 6.45; found: C, 41.45; H, 4.39; N, 6.43. ^{1}H-NMR (300 MHz, DMSO-d_6) δ_H: 15.25 (1H, CH_3–O*H*), 11.89 (2H), 7.94 (2H), 5.60 (4H), 3.34 (4H), 3.20 (6H), 3.31 (3H) (ESI Fig. S2†); selected FT-IR data (KBr, cm^{-1}), $\nu_{(OH)}$ = 3367.19 cm^{-1}, $\nu_{(C=N)}$ = 1634.26 cm^{-1}, $\nu_{(NO_3)}$ = 1462 cm^{-1} (ESI Fig. S3†); ESI-MS m/z, ion: 435.19, {[**H_5dpm** − 3H] + $2Cu^{2+}$}$^+$, $C_{15}H_{19}N_2O_5Cu_2$ (ESI Fig. S4†).

3.4. Cell culture

Vero cell (Vero 76, ATCC no. CRL-1587) lines were prepared from continuous culture in Dulbecco's modified Eagle's medium (DMEM, Sigma Chemical Co., St. Louis, MO) supplemented with 10% fetal bovine serum (Invitrogen), penicillin (100 μg mL^{-1}), and streptomycin (100 μg mL^{-1}). The Vero 76 were obtained from the American Type Culture Collection (Rockville, MD) and maintained in DMEM containing 10% (v/v) fetal bovine serum and antibiotics in a CO_2 incubator. Cells were initially propagated in 75 cm^2 polystyrene, filter-capped tissue culture flask in an atmosphere of 5% CO_2 and 95% air at 37 °C in CO_2 incubator. When the cells reached the logarithmic phase, the cell density was adjusted to 1.0×10^5 per well in culture media. The cells were then used to inoculate in a glass bottom dish, with 1.0 mL (1.0×10^4 cells) of cell suspension in each dish. After cell adhesion, culture medium was removed. The cell layer was rinsed twice with phosphate buffered saline (PBS), and then treated according to the experimental need.

3.5. Cell imaging study

For fluorescence imaging studies Vero cells, 1×10^4 cells in 1000 μL of medium, were seeded on sterile 35 mm dish, glass bottom culture dish (ibidi GmbH, Germany), and incubated at 37 °C in a CO_2 incubator for 10 hours. Then cells were washed with 500 μL PBS followed by incubation with final concentration

of 0.4 mM **H_5dpm** dissolved in 1000 μL DMEM at 37 °C for 30 min in a CO_2 incubator and washed with 500 μL phosphate buffered saline PBS (pH 7.4) to remove any free **H_5dpm**. Again 1000 μL PBS was added and observed under an Olympus IX71 microscope. Images were analyzed by Image-pro plus (version 6.3) with excitation at nearby 433 nm Enhanced Cyan FP (ECFP)-specific filter, and emit at nearby 510 nm. The cells were incubated in PBS with metal solution [$Cu(NO_3)_2 \cdot 3H_2O$] to a final concentrations of 4 mM, incubated for 30 min and images were captured.

3.6. Theoretical methods

The geometrical structures in their singlet ground state (S_0) and excited state (S_1) were optimized by DFT and time-dependent DFT (TDDFT)[71–73] methods with the BP86 functional[74] approach associated with the conductor-like polarizable continuum model (CPCM).[75–77] The geometries of the complex in their ground S_0 were optimized in solution phase. For the complex and ligand keto and enol forms) we calculated 60 singlet–singlet transition using their ground S_0 state geometries and using the conductor-like polarizable continuum model. For all atoms we have used 6-311+G* as the basis set. The calculated electronic density plots for the frontier molecular orbitals were prepared by using the GaussView 5.0 software. All the calculations were performed with the Gaussian 09 software package.[78]

3.7. Sample preparation for UV-vis and fluorescence spectral studies

Stock solutions of various metal ions were prepared in deionized water and a stock solution of **H_5dpm** was prepared in Tris-buffer solution (25 mM, pH = 7.4) with deionized water. In UV-visible titration experiment, aqueous solution of **H_5dpm** 10^{-3} (M) was filled in a quartz optical cell of 1.0 cm optical path length to achieve a final concentration of solution of **H_5dpm** 5×10^{-6} (M) in 2000 μL and metal ions were added using a micropipette to a solution of **H_5dpm**. For emission titration experiment, 10^{-3} (M) solution of **H_5dpm** 10 μL was taken in a quartz optical cell of 1.0 cm optical path length in 2000 μL and then stock solutions of metal ions were added gradually to it by using micropipette. Spectral data were recorded at 1 min after the addition of the metal ions for both titration. For fluorescence measurements, excitation was provided at 434 nm in Tris-buffer solution (25 mM, pH = 7.4), and a strong emission peak was observed at 510 nm.

3.8. Evaluation of fluorescence quantum yield in aqueous Tris-buffer solution

Fluorescence quantum yield was determined using quinine sulphate ($\Phi_R = 0.546$ in 0.1 M H_2SO_4) as standard at an excitation wavelength of 434 nm. The quantum yield is calculated using the following equation.

$$\Phi_S = \Phi_R \frac{A_S}{A_R} \times \frac{Abs_R}{Abs_S} \times \frac{{\eta_S}^2}{{\eta_R}^2}$$

where A terms denote the integrated area under the fluorescence curve, Abs denotes absorbance, η is the refractive index of the medium and Φ is the fluorescence quantum yield. Subscripts S and R denote the respective parameters for the studied sample and reference, respectively.

3.9. Determination of Cu^{2+} in aqueous Tris-buffer solution

The limit of detection (LOD) was calculated from the fluorescence titration data based on a reported and broadly used method.[79–81] In ESI Fig. S11† reveals a good linear correlation between the value of relative fluorescence ($\Delta F = F_0 - F$) and the concentration of Cu^{2+} ions with a correlation coefficient (R^2) of 0.9986. A linear regression curve was then fitted to these normalized ratio data, and the point at which this line crossed the ordinate axis was considered as the detection limit. The detection limit was calculated using the following equation.

$$DL = K \times \frac{\sigma}{S}$$

where $K = 2$ or 3 (we take 3 in this case), σ is the standard deviation of the blank solution and S is the slope of the calibration curve.

4. Results and discussion

4.1. Syntheses and general characterization

A new water soluble sensor **H_5dpm** was designed and synthesized through one step condensation of 4-methyl-2,6-diformylphenol and 3-amino-1,2-propanediol in a 1 : 2 molar ratio in methanol medium and isolated as a yellow oily compound as shown in Scheme 1 and characterized by FT-IR, ^{1}H-NMR, ^{13}C-NMR and ESI-MS method. ESI-MS study of **H_5dpm** in methanol solution exhibits an intense peak at m/z = 311.16, which can be assigned to [**H_5dpm** + H]$^+$, $C_{15}H_{23}N_2O_5$ (ESI Fig. S4†). The FT-IR spectra clearly indicate the C=N and O–H stretching band of the chemosensor **H_5dpm** appears at 1646 cm^{-1} and 3413 cm^{-1} (ESI Fig. S3†). To explore the coordinating behavior of **H_5dpm** toward 3d metal ions, **H_5dpm** was allowed to react with zinc metal ions using $Zn(OAc)_2 \cdot 2H_2O$ and NH_4SCN, in 1 : 2 : 1 molar ratio, in methanol solution. The reaction mixture was kept for slow evaporation method and yellow colored single crystals of complex **1** was separated out and the structure was authenticated using single crystal X-ray diffraction analyses. **H_5dpm** was further made to react with $Cu(NO_3)_2 \cdot 3H_2O$ in methanol solution, to afford deep green crystalline complex **2** in reasonably good yield but single crystals suitable for X-ray diffraction were not obtained even after several attempts. Besides elemental analysis, all the complexes were initially characterized by FT-IR spectra. A strong and sharp band due to the azomethine $\nu_{(C=N)}$ group appears at 1638.44 and 1634.26 cm^{-1} for complexes **1** and **2**, respectively. The sharp peak at 2078.62 cm^{-1} for complex **1** is due to the presence of thiocyanate ion. In order to establish the identity of the species present in solution, the electrospray ionization mass spectra (ESI-MS positive) of complexes **1** and **2** were recorded in methanol solution. The complex **1** exhibited the base peak at m/z = 557.02, which can be assigned to the cationic species [**H_4dpm** + $Zn_2(OAC)_2$]$^+$, $C_{19}H_{27}N_2O_9Zn_2$. The appearance of peak at m/z =

435.19, may be attributed to the presence of $\{[\mathbf{H_5dpm} - 3H] + 2Cu^{2+}\}^+$, $C_{15}H_{19}N_2O_5Cu_2$.

4.2. UV-vis spectroscopic features of H_5dpm

The UV-vis absorption spectrum of **H_5dpm** was investigated in aqueous solution of 25 mM Tris-buffer at pH 7.4 which revealed a strong band with a maximum absorbance peak at 434 nm. To pinpoint the selectivity of **H_5dpm**, chloride salts of (20 equiv.) Na^+, K^+, Ca^{2+}, Mg^{2+}, Mn^{2+}, Ba^{2+}, Fe^{2+}, Fe^{3+}, Zn^{2+}, Cd^{2+}, Hg^{2+}, Ni^{2+}, Sr^{2+}, Cu^{2+}, Co^{2+} and Al^{3+} in Tris-buffer solution (25 mM, pH = 7.4) were selected (ESI Fig. S6†). As evident from Fig. 1, a conspicuous change in UV-vis spectral pattern was manifested only in presence of Cu^{2+} in the absorption spectra of **H_5dpm**. In order to gain a quantitative insight regarding the specific interaction of Cu^{2+} and **H_5dpm**, a sequential titration of **H_5dpm** with increasing Cu^{2+} (0–10 equiv. of Cu^{2+}) was pursued. As can be seen from Fig. 1, the maximum absorption intensity at 434 nm gradually decreased and another new absorption band at 375 nm is gradually generated with solution color turning from yellowish to sky blue after addition of 10 equiv. of Cu^{2+} (Fig. 2). The binding stoichiometry between **H_5dpm** and Cu^{2+} has been investigated using the Job's method by varying concentrations of **H_5dpm** and Cu^{2+} and monitoring the change in absorption at 375 nm. The experimental results are fitted considering 2 : 1 complex formation between Cu^{2+} and **H_5dpm** (ESI Fig. S10†). The goodness of the linear fit of the Benesi–Hildebrand (B–H) plot[83] ($R^2 = 0.998$) of $1/(A_0 - A)$ *vs.* $1/[Cu^{2+}]^2$ for 2 : 1 complex formation (ESI Fig. S8†) confirms the binding stoichiometry between Cu^{2+} and **H_5dpm** with binding constant value 5.90×10^{11} M^{-2}. To characterize the **H_5dpm**–Cu^{2+} complex more intensely, ESI-MS experiment was performed which is in line with the existence 2 : 1 complexes **H_5dpm**–Cu^{2+}. In ESI-MS spectra the base line peak is for the $\{[\mathbf{H_5dpm} - 3H] + 2Cu^{2+}\}^+$. Although X-ray quality single crystals of the **H_5dpm**–Cu^{2+} complex were not obtained, we were able to obtain crystals of a dimeric Zn^{2+} complex $[\mathbf{H_4dpm} + Zn_2(OAc)_2]^+$, $(C_{19}H_{27}N_2O_9Zn_2)$ (ESI Fig. S5, Tables S1 and S2†) which reinforces the binding modes of **H_5dpm**.

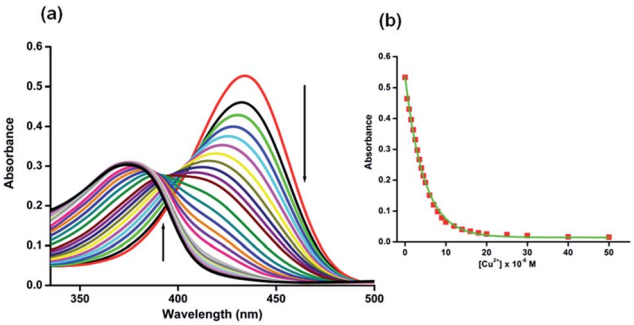

Fig. 1 Left: UV-vis spectra of **H_5dpm** (5×10^{-6} M) in Tris-buffer solution (25 mM, pH = 7.4) in the presence of various concentration of Cu^{2+} (0, 0.5, 1, 1.5, 2, 2.5, 3, 3.5, 4, 4.5, 5, 6, 7, 8, 9, 10, 12, 14, 16, 18, 20, 25, 30, 40 and 50 ($\times 10^{-6}$) M. Upward arrow indicates gradual increase of absorption at 375 nm wavelength while downward arrow indicates gradual decrease in absorption at 434 nm wavelength with increasing concentration of Cu^{2+}. Right: The absorption of **H_5dpm** at 434 nm as a function of $[Cu^{2+}]$ in Tris buffer solution (25 mM, pH = 7.4).

Thus, application of the probe **H_5dpm** renders naked eye detection of Cu^{2+} in aqueous solution (Tris-buffer, pH 7.4) (Fig. 2).

4.3. Fluorescence spectroscopic response of H_5dpm

The fluorescence spectrum of **H_5dpm** shows a strong emission band at 510 nm ($\lambda_{ex} = 434$ nm) with a high quantum yield ($\Phi = 0.248$). To explore the utility of **H_5dpm** as a simple sensing system for metal ions in aqueous solution (25 mM Tris-buffer at pH 7.4), nitrate/chloride salts of various cations (20 equiv.) were used and fluorescence spectra were recorded. No change in emission is observed for Na^+, K^+, Ca^{2+}, Mg^{2+}, Mn^{2+}, Ba^{2+}, Fe^{2+}, Fe^{3+}, Zn^{2+}, Cd^{2+}, Hg^{2+}, Ni^{2+}, Sr^{2+}, Cu^{2+}, Co^{2+} and Al^{3+} (ESI Fig. S14†). However, a significant quenching ($\Phi = 0.035$) is evident for Cu^{2+} with an insignificant interference from Co^{2+}. To get further insight into the sensing characteristics of **H_5dpm** toward Cu^{2+}, the fluorescence titration experiments were performed by incremental addition of Cu^{2+} (0–50 μM) to **H_5dpm** (5 μM) (Fig. 3). The fluorescence intensity decreased gradually with the addition of increasing amount of Cu^{2+}.[82] Competitive studies were also carried out for mixtures of Cu^{2+} and 20 equiv. of other metal ions, and the predominating quenching

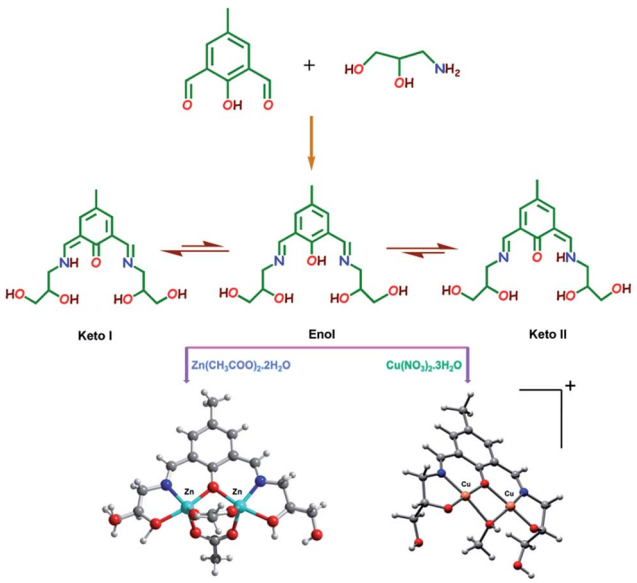

Scheme 1 Synthetic scheme for the synthesis of chemosensor (**H_5dpm**), zinc complex **1** and copper complex **2**.

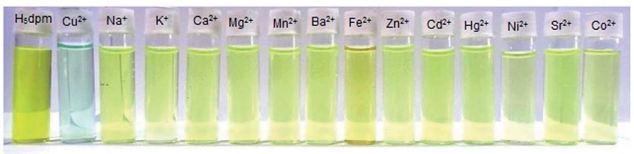

Fig. 2 Visual color change from yellow to sky blue on addition of Cu^{2+} ion in the aqueous solution of **H_5dpm** among different cations.

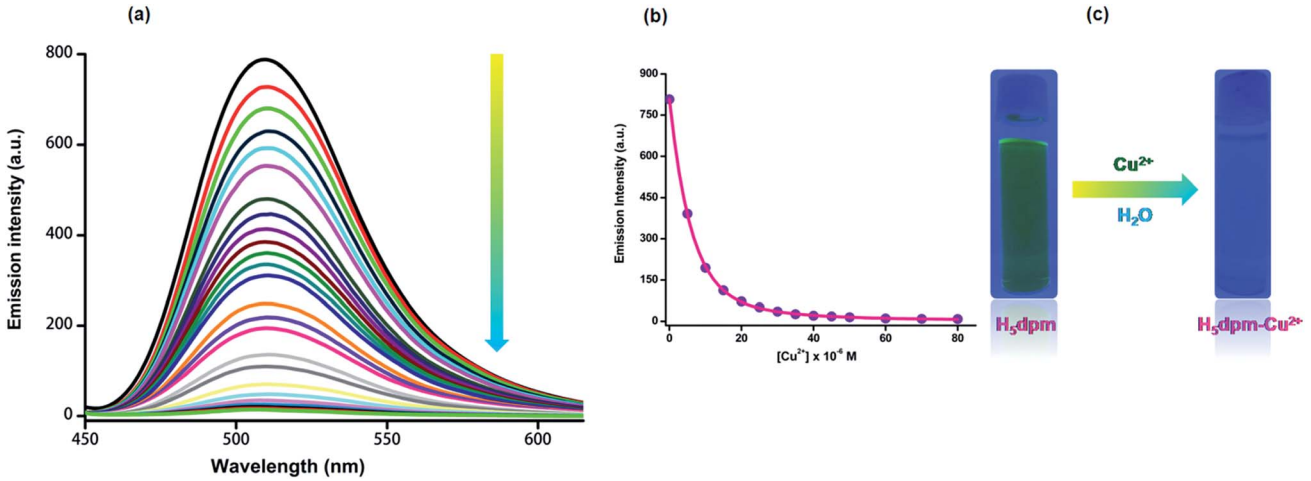

Fig. 3 (a) Fluorescence spectra of H_5**dpm** (5×10^{-6} M) with addition of increasing amount of Cu^{2+} (0, 0.5, 1, 1.5, 2, 2.5, 3, 3.5, 4, 4.5, 5, 5.5, 6, 6.5, 7, 8, 9, 10, 11, 13, 15, 20, 25, 30, 35, 40, 45 and 50 μM) in Tris-buffer (25 mM, pH = 7.4) solution. (b) Fluorescence emission intensity of H_5**dpm** as a function of [Cu^{2+}] at 510 nm (λ_{ex} = 434 nm, λ_{em} = 510 nm, slit: 5 nm/5 nm). (c) Colour change in the emission intensity addition of Cu^{2+} ion in the H_5**dpm** solution under a UV lamp (366 nm).

response was again seen only for Cu^{2+} (Fig. 4). The fluorescence responses of **H_5dpm** toward Cu^{2+} were pH-dependent, and the maximal signal was observed in the pH range of 5–11 (ESI Fig. S16†). This indicated that **H_5dpm** could be employed to detect Cu^{2+} in quite a wide pH range.

The binding constant between **H_5dpm** and Cu^{2+} derived from the fluorescence titration data using B–H equation[83] (R^2 = 0.997) was found to be 4.99×10^{11} M^{-2} (ESI Fig. S9†) and the limit of detection (LOD) was estimated to be 11.2 nM for Cu^{2+} ion in solution (ESI Fig. S11†). Noticeably, we also observed anion independency of selective Cu^{2+} detection by experimenting with $Cu(NO_3)_2$, $CuCl_2$, $Cu(CH_3COO)_2$, $Cu(SO_4)_2$ and $Cu(ClO_4)_2$ (ESI Fig. S7 and S15†). Both the absorption (434 and 375 nm) and emission (510 nm) intensities of **H_5dpm** can be reversibly switched by alternating addition of Cu^{2+}/Na_2H_2EDTA, enabling **H_5dpm** a reversible Cu^{2+} sensor (ESI Fig. S12 and S13†).

The fluorescence quenching phenomenon may be attributed to the reverse photo-induced electron transfer (reverse PET) from 4-methylphenyl moiety to the phenolic–OH and imine nitrogen because of the decrease in electron density upon complexation with Cu^{2+} (Scheme 2).[58,69,84]

As evident from Schemes 1 and 2, the probe **H_5dpm** contains abundant hydroxyl and imino groups making the probe susceptible to hydrogen bonding interactions. Therefore, we can presume that the spectral signature would be significantly affected by solvent polarity. Thus, we have studied the whole phenomenon in different media by varying the polarity of the solvent used (DMSO, DMF, acetonitrile, THF, ethanol, methanol and H_2O) to rationalize the solvent–solute interactions. Linear Solvation Energy Relationships (LSERs) are used in order

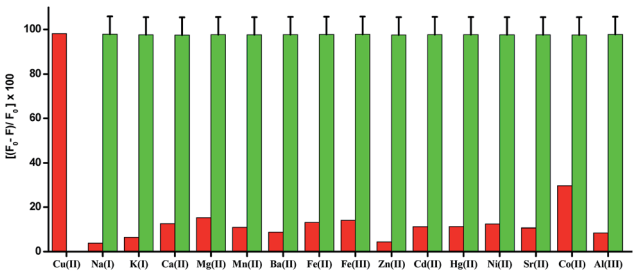

Fig. 4 Fluorescence Quenching Efficiency (FQE) of H_5**dpm** (5×10^{-6} M) in Tris buffer solution (25 mM, pH = 7.4) in the presence of 100 μM of different types of metal ions except Cu^{2+} (50 μM) as a bar graph [the red bar portion]. Fluorescence Quenching Efficiency (FQE) of a mixture of H_5**dpm** (5×10^{-6} M) solution with other metal ions (100 μM) followed by addition of 50 μM Cu^{2+} to the solution [the green bar portion] (λ_{ex} = 434 nm, λ_{em} = 510 nm, slit: 5 nm/5 nm).

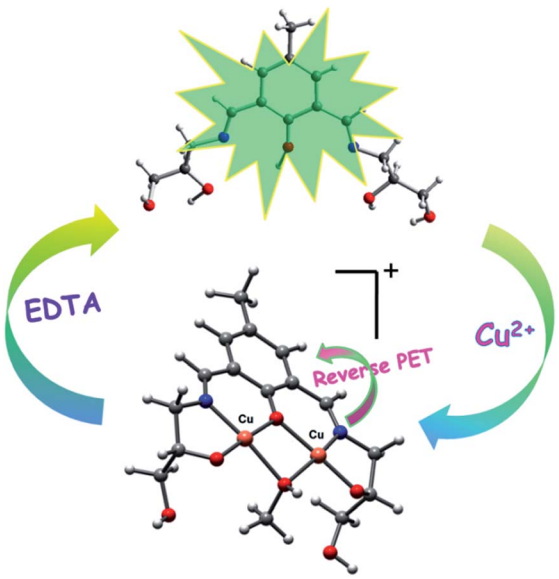

Scheme 2 Schematic illustration of proposed mechanism for the fluorescence changes of chemosensor (H_5**dpm**) upon addition of Cu^{2+}.

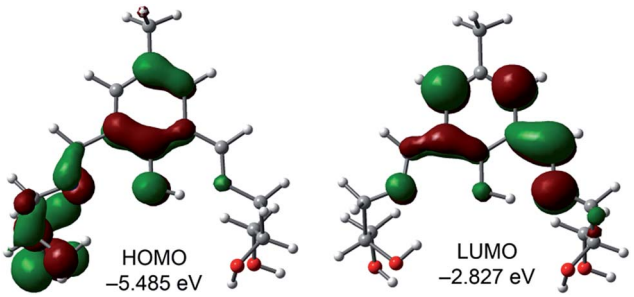

Fig. 5 Frontier orbitals of the enol form of H_5dpm.

to quantify the importance of specific and non-specific interactions[85,86] (ESI Fig. S17, S18 and S19†). From ESI Fig. S17,† it is clear that blue shift occurs with increasing solvent polarity. We have further employed Kamlet–Taft–Abboud[86] equation and calculated the relative contributions of each of the parameters (ESI Fig. S18 and S19†) which indicates significant hydrogen bonding interactions with hydrogen bond donor (HBD) and hydrogen bond acceptor (HBA) solvents as expected from the structure of the probe. ESI Fig. S19† corresponds to blue shift with increasing HBA basicity of solvents. This means that the energy difference between the ground and excited state of the **H_5dpm** increases when the HBA strength of the solvents increases.

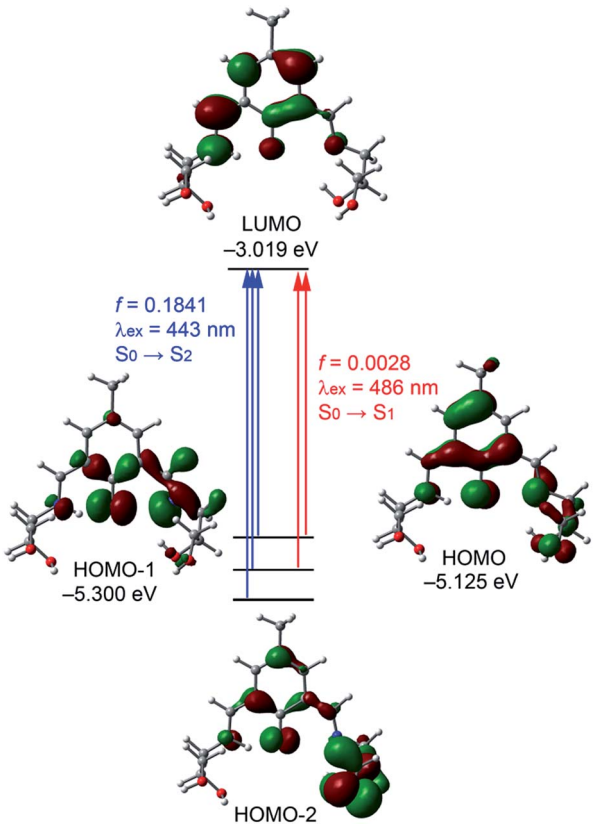

Fig. 6 Frontier molecular orbitals involved in the UV-vis absorption of the keto form of H_5dpm in two representative electronic transitions.

4.4. Computational studies of chemosensor (H_5dpm) and H_5dpm–Cu^{2+} complex

To understand the keto–enol switching mechanism prevalent in **H_5dpm**, we have theoretically investigated the phenomenon using density functional theory (DFT) method and time-dependent DFT (TDDFT) methods with the BP86 functional approach associated with the conductor-like polarizable continuum model (CPCM).

4.4.1. Chemosensor (H_5dpm). The UV-vis absorption spectrum of the **H_5dpm** used in this present work was studied at room temperature in MeOH. Experimentally **H_5dpm** shows an intense peak centered at 430 nm. The absorption energies associated with the oscillator strengths, the main configurations and the assignments calculated using the TDDFT method using the S_0 geometry for **H_5dpm** was studied using the two possible tautomeric forms (Scheme 1), since the experimental UV spectrum of the ligand may be a mixture of the absorption bands of both tautomers at room temperature because the difference in energy is small (the keto form is 1.1 kcal mol^{-1} more stable in MeOH). The results are given in ESI Tables S3 and S4† (*vide infra*).

4.4.2. Enol form of chemosensor (H_5dpm). In the ground state (S_0) the HOMO is basically composed by the phenolic aromatic moiety and the conjugated C=N bond that does not participates in the intramolecular H-bond. The LUMO is basically composed by the phenolic aromatic moiety and the conjugated C=N bond that participates in the intramolecular H-bond (Fig. 5). The energy difference between the HOMO and LUMO is 2.658 eV. The theoretical absorption band (TD-DFT calculations) is located at 387 nm ($f = 0.1114$) that is assigned to the $S_0 \rightarrow S_1$ transition. This band does not agree well with the experimental one ($\lambda_{exp} = 430$ nm), which likely suggests that the enol form is not dominant in solution.

4.4.3. Keto form of chemosensor (H_5dpm). In the ground state (S_0) the HOMO is basically composed by the six-membered keto ring, the conjugated exocyclic C=C bond, the lone pair of

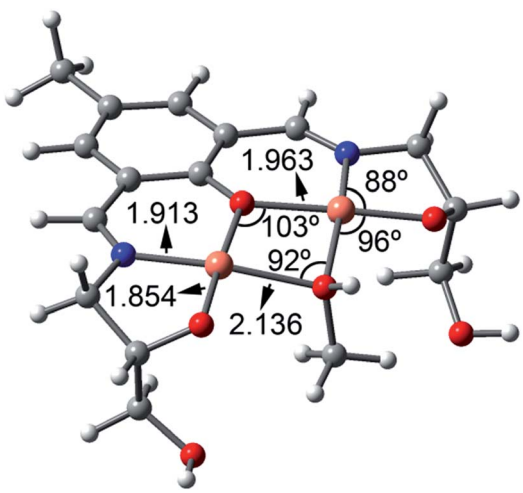

Fig. 7 BP86-D3/def2-TZVP optimized structure of $[Cu_2(H_2dpm)MeOH]^+$ complex. Distances are in Å.

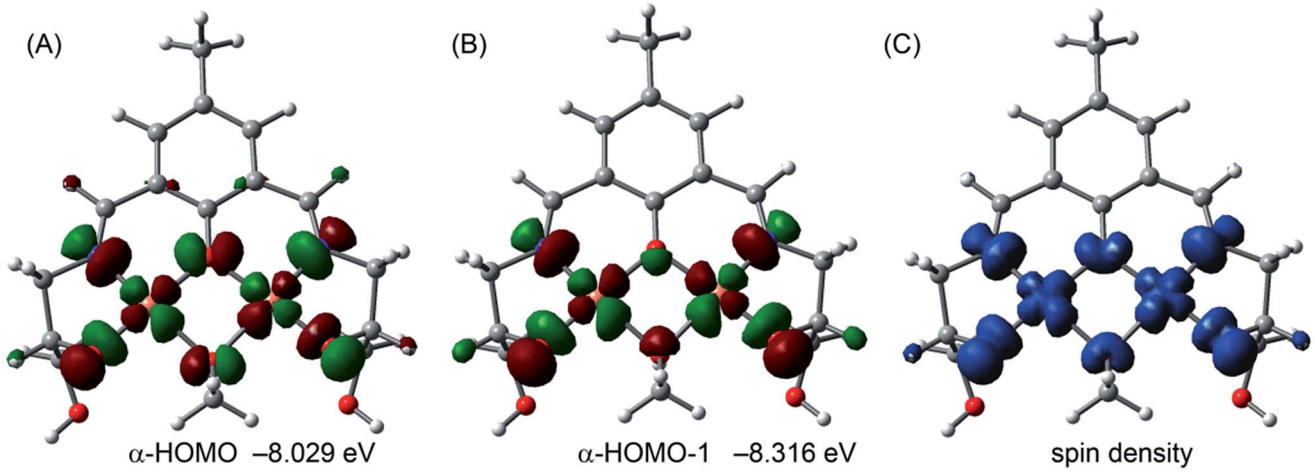

Fig. 8 Molecular orbital and spin density plots obtained for complex **2**.

the sp^3-nitrogen atom and the oxygen atom of the keto group. The HOMO−1 and HOMO−2, are stabilized by 0.175 and 0.365 eV compared to the HOMO, respectively. Similarly the LUMO is basically composed by the six-membered keto ring, the exocyclic C=C bond, the lone pair of the sp^3-nitrogen atom and the oxygen atom of the keto group. The energy difference between the HOMO and LUMO is 2.106 eV. The first calculated absorption band ($S_0 \rightarrow S_1$) is located at 489 nm for the keto form of **H_5dpm** (Fig. 6 and ESI Table S3†) and is composed by HOMO → LUMO and HOMO−1 → LUMO transitions. However this absorption band has a negligible oscillator strength (f = 0.0028) in agreement with the experimental UV spectrum. A strong absorption band ($S_0 \rightarrow S_2$) is found in the theoretical spectrum at 443 nm, which is in reasonable agreement with the experimental absorption value (430 nm). Therefore, the keto form is likely dominant in solution, in agreement with the keto–enol energetic difference (*vide supra*). This absorption band ($S_0 \rightarrow S_2$ transition) is the result of three excitations (HOMO → LUMO, HOMO−1 → LUMO, and HOMO−2 → LUMO, see ESI Table S3† and Fig. 6).

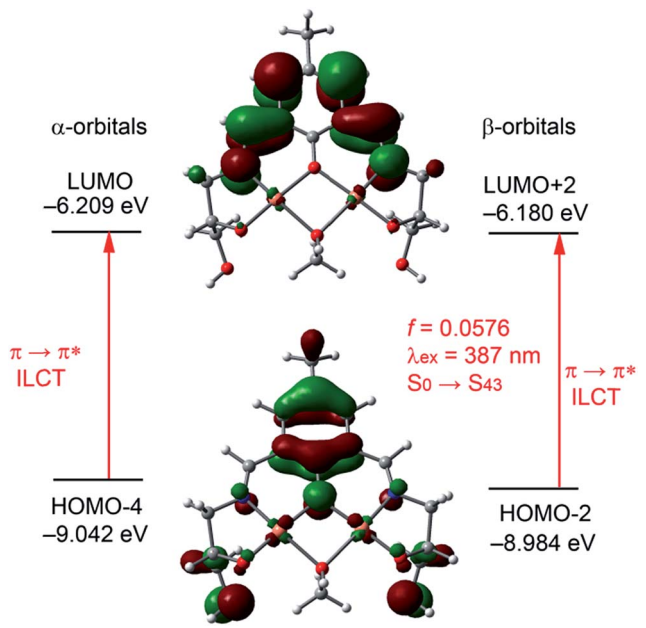

Fig. 9 Molecular orbitals involved in the lowest lying observable UV-vis absorption of the complex **2**.

4.4.4. H_5dpm–Cu^{2+} complex. We have optimized the Cu^{2+} complex of **H_5dpm** using M : L = 2 : 1 stoichiometry, since it has been evidenced experimentally by the ESI-MS experiment. A coordinated MeOH molecule (bridging ligand) has been also included in the calculation to fulfill the coordination sphere of both copper centers as indicated by the ^{1}H-NMR output (ESI Fig. S2†). The minimum energy structure along with some geometric features is shown in Fig. 7. The O–Cu distances involving the MeOH are longer than those involving the alkoxido and phenoxido groups. Since the UV-vis absorption experiments have been performed in water, we have also considered the possibility of having a water molecule instead of a MeOH as a bridging ligand. Both the geometry of the complex and orbital/spin density plots are almost identical, thus supporting the theoretical discussion (ESI Fig. S20 and S21†).

In the ground state (S_0) of the complex the HOMO and HOMO−1 are mainly composed by the Cu^{2+} magnetic orbitals ($d_{x^2-y^2}$) and some contribution of the atoms of the ligand that are directly bonded to the metal centers (Fig. 8). In fact the spin density plot for the high spin configuration (ferromagnetic coupling) clearly indicates that the spin is located in the Cu metal centers and the atoms directly bonded to them (Fig. 8C).

The α-LUMO (Fig. 9) is basically composed by the phenolic aromatic moiety and both conjugated C=N exocyclic bonds. The energy difference between the α-HOMO and α-LUMO is 1.820 eV. To get better insight into the experimental UV-absorption value TDDFT calculations were done for the complex on the basis of the optimized geometry. The calculated absorption energy associated with its oscillator strength, the main configurations and their assignments of the complex are given in ESI Table S4.† Only one distinguishable singlet → singlet absorption band is found at 387 nm (3.1992 eV and f =

0.0576), which can be mainly attributed (only those contributions higher than 10% are listed in ESI Table S4†) to a combination of the HOMO−4 → LUMO (alpha) and HOMO−13 → LUMO (beta) and HOMO−2 → LUMO+2 (beta) transitions. The HOMO−4 → LUMO (alpha) and HOMO−2 → LUMO+2 (beta) transition are formally equivalent (since the high spin configuration for the Cu(II) complex is used) and can be assigned to $\pi(L) \rightarrow \pi^*(L)$ transitions with ILCT character, (Fig. 9). The experimental value is in reasonable agreement with the theoretical one (overestimated in 12 nm), giving reliability to the proposed structure of the complex with the bridging MeOH molecule. For completeness, we have also performed the calculations of the absorption bands using water as solvent. The results are given in ESI Table S4† and they are very similar to those given for the MeOH complex.

4.5. Application of H_5dpm for Cu^{2+} detection in Vero cells

In vitro fluorescence imaging of biological systems is at the forefront of research on optical imaging techniques for biomedical applications. As **H_5dpm** interacts with Cu^{2+}, and the resulting stable complex shows switch-off fluorescence in visible region, it became crucial to assess the effectiveness of **H_5dpm** as a probe for intracellular presence of Cu^{2+} by fluorescence microscopy. Fluorescence microscopic studies revealed fluorescence for Vero cells when treated with **H_5dpm** (Fig. 10). Upon incubation with **H_5dpm** followed by Cu^{2+} solution, a switch-off fluorescence was observed inside Vero cells. The fluorescence microscopic analysis strongly suggested that both **H_5dpm** and Cu^{2+} could readily cross the membrane barrier of the Vero cells. It is significant to mention here that bright field images of treated cells did not reveal any gross morphological changes, which suggested that Vero cells were viable. These findings open up a new avenue for future *in vitro* biomedical applications of **H_5dpm**.

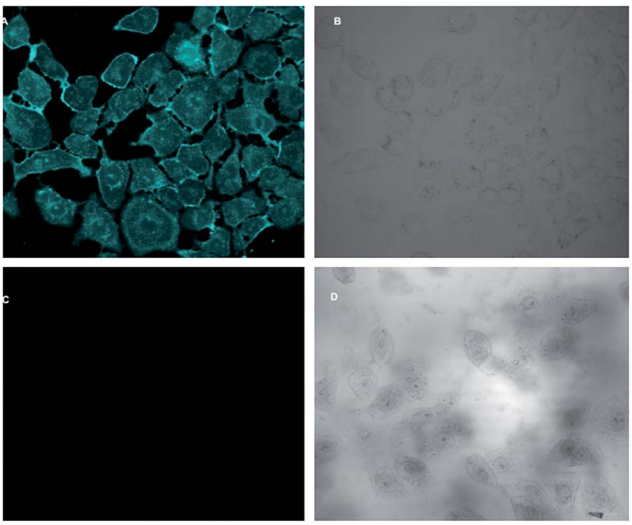

Fig. 10 Fluorescence microscopic images in Vero 76 cells: (A) image of the cells, pretreated with H_5dpm at 0.4 mM concentration, (B) bright field with H_5dpm at 0.4 mM concentration, (C) image of the cells treated with H_5dpm followed by metal [$Cu(NO_3)_2 \cdot 3H_2O$] at concentration 4 mM, (D) bright field image of the cells treated with H_5dpm followed by metal [$Cu(NO_3)_2 \cdot 3H_2O$] at concentration 4 mM, and switch-off fluorescence signal is observed. All images were acquired with a 40× objective lens.

5. Conclusion

In conclusion, we have developed a new chemosensor, **H_5dpm**, based on simple condensation of 4-methyl-2,6-diformylphenol and 3-amino-1,2-propanediol which enables selective colorimetric naked eye detection of Cu^{2+} in aqueous solution. In the absence of Cu^{2+}, **H_5dpm** displays fluorescence emission at 510 nm, and on addition of Cu^{2+}, **H_5dpm** shows significant fluorescence quenching as a result of reverse PET effect. **H_5dpm** demonstrated remarkable selectivity and specificity towards Cu^{2+} in aqueous solution under physiological conditions with detection limit of 11.2 nM. The reported probe is only the third diformyl phenol based system in literature that exhibits selective colorimetric and fluorometric detection of Cu^{2+}. Theoretical studies were performed to establish the underlying keto–enol tautomerism. **H_5dpm** also allowed for *in vitro* imaging of Cu^{2+} in Vero cells. Hence, **H_5dpm** represents a highly promising and biomedically applicable probe for colorimetric, fluorometric and rapid detection of Cu^{2+} in aqueous solution and its monitoring *in vitro*.

Acknowledgements

B. Naskar acknowledge UGC, India for fellowship (sanction no. RGNF-2013-14-SC-WES-38844). RFSMS fellowship (Sanction No. UGC/740/RFSMS) to R. Modak and is gratefully acknowledge. DST-FIST is acknowledged for providing Single crystal XRD at department of Chemistry, University of Calcutta. A. B. and A. F. thank DGICYT of Spain (projects CTQ2014-57393-C2-1-P and CONSOLIDER INGENIO CSD2010-00065, FEDER funds) for funding. We thank the CTI (UIB) for free allocation of computer time. We sincerely thank Soumen Ghosh and Aniruddha Ganguly of University of Calcutta, Kolkata, for their helpful suggestions.

Notes and references

1 S. J. Lippard and J. M. Berg, *Principles of Bioinorganic Chemistry*, University ScienceBooks, Mill Valley, CA, 1994.
2 M. L. Turski and D. J. Thiele, *J. Biol. Chem.*, 2009, **284**, 717–721.
3 L. Banci, I. Bertini, S. Ciofi-Baffoni, T. Kozyreva, K. Zovo and P. Paulmaa, *Nature*, 2010, **465**, 645–648.
4 E. L. Que, D. W. Domaille and C. J. Chang, *Chem. Rev.*, 2008, **108**, 1517–1549.
5 H. Kozlowski, A. J. Klos, J. Brasun, E. Gaggelli, D. Valensin and G. Valensin, *Coord. Chem. Rev.*, 2009, **253**, 2665–2685.
6 E. Gaggelli, H. Kozlowski, D. Valensin and G. Valensin, *Chem. Rev.*, 2006, **106**, 1995–2044.
7 T. V. O. Halloran and V. C. Culotta, *J. Biol. Chem.*, 2000, **275**, 25057–25060.

8 A. C. Rosenzweig and T. V. O. Halloran, *Curr. Opin. Chem. Biol.*, 2000, **4**, 140–147.
9 A. Singh, Q. Yao, L. Tong, W. C. Still and D. Sames, *Tetrahedron Lett.*, 2000, **41**, 9601–9605.
10 S. Puig and D. J. Thiele, *Curr. Opin. Chem. Biol.*, 2002, **6**, 171–180.
11 F. Arnesano, L. Banci, I. Bertini and S. C. Baffoni, *Eur. J. Inorg. Chem.*, 2004, 1583–1593.
12 D. Y. Sasaki, D. R. Shnek, D. W. Pack and F. H. Arnold, *Angew. Chem., Int. Ed.*, 1995, **34**, 905–907.
13 R. Kramer, *Angew. Chem., Int. Ed.*, 1998, **37**, 772–773.
14 A. Torrado, G. K. Walkup and B. Imperiali, *J. Am. Chem. Soc.*, 1998, **120**, 609–610.
15 P. Grandini, F. Mancin, P. Tecilla, P. Scrimin and U. Tonellato, *Angew. Chem., Int. Ed.*, 1999, **38**, 3061–3064.
16 R. Uauy, A. Maass and M. Araya, *Am. J. Clin. Nutr.*, 2008, **88**, 867S–871S.
17 Z. C. Xu, Y. Xiao, X. H. Qian, J. N. Cui and D. W. Cui, *Org. Lett.*, 2005, **7**, 889.
18 R. Seth, S. Yang, S. Choi, M. Sabean and E. A. Roberts, *Toxicol. in Vitro*, 2004, **18**, 501.
19 D. J. Waggoner, T. B. Bartnikas and J. D. Gitlin, *Neurobiol. Dis.*, 1999, **6**, 221.
20 J. F. B. Mercer, *Trends Mol. Med.*, 2001, **7**, 64.
21 D. R. Brown and H. Kozlowski, *Dalton Trans.*, 2004, **13**, 1907–1917.
22 D. Huster and S. Lutsenko, *Mol. BioSyst.*, 2007, **3**, 816.
23 D. Strausak, J. F. B. Mercer, H. H. Dieter, W. Stremmel and G. Multhaup, *Brain Res. Bull.*, 2001, **55**, 175–185.
24 J. Valentine and P. J. Hart, *Proc. Natl. Acad. Sci. U. S. A.*, 2003, **100**, 3617–3622.
25 G. L. Millhauser, *Acc. Chem. Res.*, 2004, **37**, 79–85.
26 D. R. Brown and H. Kozlowski, *Dalton Trans.*, 2004, 1907–1917.
27 H. Küpper and P. M. H. Kroneck, *Heavy Metal Uptake by Plants and Cyanobacteria*, 2005, vol. 44, pp. 97–144.
28 E. Gaggelli, H. Kozlowski, D. Valensin and G. Valensin, *Chem. Rev.*, 2006, **106**, 1995–2044.
29 S. Krupanidhi, A. Sreekumar and C. B. Sanjeevi, *Indian J. Med. Res.*, 2008, **128**, 448–461.
30 S. V. Wegner, H. Arslan, M. Sunbul, J. Yin and C. He, *J. Am. Chem. Soc.*, 2010, **132**, 2567–2569.
31 C. Vulpe, B. Levinson, S. Whitney, S. Packman and J. Gitschier, *Nat. Genet.*, 1993, **3**, 7–13.
32 D. J. Waggoner, T. B. Bartnikas and J. D. Gitlin, *Neurobiol. Dis.*, 1999, **6**, 221–230.
33 J. S. Valentine and P. J. Hart, *Proc. Natl. Acad. Sci. U. S. A.*, 2003, **100**, 3617–3622.
34 D. R. Brown and H. Kozlowski, *Dalton Trans.*, 2004, 1907–1917.
35 K. J. Barnham, C. L. Masters and A. I. Bush, *Nat. Rev. Drug Discovery*, 2004, **3**, 205–214.
36 B. E. Kim, T. Nevitt and D. J. Thiele, *Nat. Chem. Biol.*, 2008, **4**, 176–185.
37 G. J. Brewer, *Curr. Opin. Chem. Biol.*, 2003, **7**, 207–212.
38 S. P. Leach, M. D. Salman and D. Hamar, *Anim. Health Res. Rev.*, 2006, **7**, 97–105.
39 K. J. Barnham and A. I. Bush, *Curr. Opin. Chem. Biol.*, 2008, **12**, 222–228.
40 R. R. Crichton, D. T. Dexter and R. J. Ward, *Coord. Chem. Rev.*, 2008, **252**, 1189–1199.
41 M. C. Linder and M. H. Azam, *Am. J. Clin. Nutr.*, 1996, **63**, 797S–811S.
42 U. Forstnerand and G. T. Wittmann, *Metal Pollution in the Aquatic Environment*, Springer, Berlin, Heidelberg, New York, 1981, p. 8.
43 E. Merian, *Analysis and Biological Relevance*, VCH, Weinheim, 1991, p. 893.
44 E. Merian, *Metals and Their Compounds in the Environment*, VCH, Weinheim, Germany, 1991.
45 D. W. Domaille, E. L. Que and C. J. Chang, *Nat. Chem. Biol.*, 2008, **4**, 168.
46 Y. Liu, P. Liang and L. Guo, *Talanta*, 2005, **68**, 25–30.
47 A. A. Ensafi, T. Khayamian and A. Benvidi, *Anal. Chim. Acta*, 2006, **561**, 225–232.
48 A. P. S. Gonzales, M. A. Firmino, C. S. Nomura, F. R. P. Rocha, P. V. Oliveira and I. Gaubeur, *Anal. Chim. Acta*, 2009, **636**, 198–204.
49 S.-P. Wu, T.-H. Wang and S.-R. Liu, *Tetrahedron*, 2010, **66**, 9655–9658.
50 D. Maity and T. Govindaraju, *Chem.–Eur. J.*, 2011, **17**, 1410–1414.
51 T. Li, Z. Yang, Y. Li, Z. Liu, G. Qi and B. Wang, *Dyes Pigm.*, 2011, **88**, 103–108.
52 P. Kaur, D. Sareen and K. Singh, *Talanta*, 2011, **83**, 1695–1700.
53 Y. Xiang, A. Tong, P. Jin and Y. Ju, *Org. Lett.*, 2006, **8**, 2863–2866.
54 H. S. Jung, P. S. Kwon, J. W. Lee, J. Kim, C. S. Hong, J. W. Kim, S. Yan, J. Y. Lee, J. H. Lee, T. Joo and J. S. Kim, *J. Am. Chem. Soc.*, 2009, **131**, 2008–2012.
55 R. Sheng, P. Wang, Y. Gao, Y. Wu, W. Liu, J. Ma, H. Li and S. Wu, *Org. Lett.*, 2008, **10**, 5015–5018.
56 L. Yuan, W. Lin, B. Chen and Y. Xie, *Org. Lett.*, 2012, **14**, 432–435.
57 A. Kumar, V. Kumar, U. Diwan and K. K. Upadhyay, *Sens. Actuators, B*, 2013, **176**, 420–427.
58 V. Chandrasekhar, S. Das, R. Yadav, S. Hossain, R. Parihar, G. Subramanium and P. Sen, *Inorg. Chem.*, 2012, **51**, 8664–8666.
59 R. Bergonzi, L. Fabbrizzi, M. Licchelli and C. Mangano, *Coord. Chem. Rev.*, 1998, **170**, 31–46.
60 Z. C. Liu, Z. Y. Yang, T. R. Li, B. D. Wang, Y. Li, D. D. Qin, M. F. Wang and M. H. Yan, *Dalton Trans.*, 2011, **40**, 9370–9373.
61 S. H. Kim, J. S. Kim, S. M. Park and S. K. Chang, *Org. Lett.*, 2006, **8**, 371–374.
62 S. Khatua, S. H. Choi, J. Lee, J. O. Huh, Y. Do and D. G. Churchill, *Inorg. Chem.*, 2009, **48**, 1799–1801.
63 (*a*) B. Naskar, R. Modak, Y. Sikdar, D. K. Maiti, A. Banik, T. K. Dangar, S. Mukhopadhyay, D. Mandal and S. Goswami, *J. Photochem. Photobiol., A*, 2016, **321**, 99–109; (*b*) B. Naskar, R. Modak, Y. Sikdar, D. K. Maiti, A. Bauzá, A. Frontera, A. Katarkar, K. Chaudhuri and S. Goswami,

Sens. Actuators, B, 2017, **239**, 1194–1204; (*c*) S. Mandal, Y. Sikdar, D. K. Maiti, G. P. Maiti, S. K. Mandal, J. K. Biswas and S. Goswami, *RSC Adv.*, 2015, **5**, 72659–72669.

64 S. Lohar, S. Pal, B. Sen, M. Mukherjee, S. Banerjee and P. Chattopadhyay, *Anal. Chem.*, 2014, **86**, 11357–11361.

65 A. Gogoi, S. Mukherjee, A. Ramesh and G. Das, *Anal. Chem.*, 2015, **87**, 6974–6979.

66 S. Anbu, S. Kamalraj, C. Jayabaskaran and P. S. Mukherjee, *Inorg. Chem.*, 2013, **52**, 8294–8296.

67 U. C. Saha, B. Chattopadhyay, K. Dhara, S. K. Mandal, S. Sarkar, A. R. K. Bukhsh, M. Mukherjee, M. Helliwell and P. Chattopadhyay, *Inorg. Chem.*, 2011, **50**, 1213–1219.

68 P. Roy, K. Dhara, M. Manassero, J. Ratha and P. Banerjee, *Inorg. Chem.*, 2007, **46**, 6405–6412.

69 S. Anbu, R. Ravishankaran, M. F. C. G. d. Silva, A. A. Karande and A. J. L. Pombeiro, *Inorg. Chem.*, 2014, **53**, 6655–6664.

70 R. R. Gagne, C. L. Spiro, T. J. Smith, C. A. Hamann, W. R. Thies and A. K. Shiemke, *J. Am. Chem. Soc.*, 1981, **103**, 4073.

71 M. E. Casida, C. Jamoroski, K. C. Casida and D. R. Salahub, *J. Chem. Phys.*, 1998, **108**, 4439–4449.

72 R. E. Stratmann, G. E. Scuseria and M. J. Frisch, *J. Chem. Phys.*, 1998, **109**, 8218–8224.

73 R. Bauernschmitt and R. Ahlrichs, *Chem. Phys. Lett.*, 1996, **256**, 454–464.

74 J. P. Perdew, *Phys. Rev. B: Condens. Matter Mater. Phys.*, 1986, **33**, 8822–8824.

75 M. Cossi, N. Rega, G. Scalmani and V. Barone, *J. Comput. Chem.*, 2003, **24**, 669–681.

76 M. Cossi and V. Barone, *J. Chem. Phys.*, 2001, **115**, 4708–4717.

77 V. Barone and M. Cossi, *J. Phys. Chem. A*, 1998, **102**, 1995–2001.

78 M. J. Frisch, G. W. Trucks, H. B. Schlegel, G. E. Scuseria, M. A. Robb, J. R. Cheeseman, G. Scalmani, V. Barone, B. Mennucci, G. A. Petersson, H. Nakatsuji, M. Caricato, X. Li, H. P. Hratchian, A. F. Izmaylov, J. Bloino, G. Zheng, J. L. Sonnenberg, M. Hada, M. Ehara, K. Toyota, R. Fukuda, J. Hasegawa, M. Ishida, T. Nakajima, Y. Honda, O. Kitao, H. Nakai, T. Vreven, J. A. Montgomery Jr, J. E. Peralta, F. Ogliaro, M. Bearpark, J. J. Heyd, E. Brothers, K. N. Kudin, V. N. Staroverov, R. Kobayashi, J. Normand, K. Raghavachari, A. Rendell, J. C. Burant, S. S. Iyengar, J. Tomasi, M. Cossi, N. Rega, J. M. Millam, M. Klene, J. E. Knox, J. B. Cross, V. Bakken, C. Adamo, J. Jaramillo, R. Gomperts, R. E. Stratmann, O. Yazyev, A. J. Austin, R. Cammi, C. Pomelli, J. W. Ochterski, R. L. Martin, K. Morokuma, V. G. Zakrzewski, G. A. Voth, P. Salvador, J. J. Dannenberg, S. Dapprich, A. D. Daniels, Ö. Farkas, J. B. Foresman, J. V. Ortiz, J. Cioslowski and D. J. Fox, *Gaussian 09, Revision B.01*, Gaussian, Inc., Wallingford, CT, 2009.

79 M. Shortreed, R. Kopelman, M. Kuhn and B. Hoyland, *Anal. Chem.*, 1996, **68**, 1414.

80 A. Caballero, R. Martínez, V. Lloveras, I. Ratera, J. Vidal-Gancedo, K. Wurst, A. Tárraga, P. Molina and J. Veciana, *J. Am. Chem. Soc.*, 2005, **127**, 15666.

81 (*a*) W. Y. Lin, L. Yuan, Z. M. Cao, Y. M. Feng and L. L. Long, *Chem.–Eur. J.*, 2009, **15**, 5096; (*b*) L. Rosa-Romo, M. T. Oropeza-Guzman, A. Olivas-Sarabia and G. Pina-Luis, *Sens. Actuators, B*, 2016, **233**, 459–468; (*c*) Q. Wu and E. V. Anslyn, *J. Am. Chem. Soc.*, 2004, **126**, 14682–14683; (*d*) T. Gunnlaugsson, J. P. Leonard and N. S. Murray, *Org. Lett.*, 2004, **6**, 1557–1560; (*e*) H. Qin, J. Ren, J. Wang and E. Wang, *Chem. Commun.*, 2010, **46**, 7385–7387.

82 M. H. Lim, B. A. Wong, W. H. Pitcock Jr, D. Mokshagundam, M. H. Baik and S. J. Lippard, *J. Am. Chem. Soc.*, 2006, **128**, 14364.

83 H. Lineweaver and D. Burk, *J. Am. Chem. Soc.*, 1934, **56**, 658.

84 M. Kumar, R. Kumar, V. Bhalla, P. R. Sharma, T. Kaurb and Y. Qurish, *Dalton Trans.*, 2012, **41**, 408.

85 (*a*) R. W. Taft, J. L. M. Abboud, M. I. Kamlet and M. H. Abraham, *J. Solution Chem.*, 1985, **14**, 153–156; (*b*) M. D. Trone and M. G. Khaledi, *J. Chromatogr. A*, 2000, **886**, 245–257; (*c*) M. J. Kamlet, J. L. M. Abboud and R. W. Taft, *Prog. Phys. Org. Chem.*, 1981, **13**, 485–630; (*d*) A. L. Revelli, F. Mutelet and J. N. Jaubert, *Ind. Eng. Chem. Res.*, 2010, **49**, 3883–3892.

86 (*a*) R. Papadakis, I. Deligkiozi and A. Tsolomitis, *Anal. Bioanal. Chem.*, 2010, **397**, 2253–2259; (*b*) T. M. Krygowski and W. R. Fawcett, *J. Am. Chem. Soc.*, 1975, **97**, 2143–2148.